



Article

Thermoelectric Properties of Reduced Graphene Oxide/Bi₂Te₃ Nanocomposites

Yong Du ^{1,*} , Jia Li ¹, Jiayue Xu ¹ and Per Eklund ² 

¹ School of Materials Science and Engineering, Shanghai Institute of Technology, 100 Haiquan Road, Shanghai 201418, China; 166081106@mail.sit.edu.cn (J.L.); xujiayue@sit.edu.cn (J.X.)

² Thin Film Physics Division, Department of Physics, Chemistry and Biology (IFM), Linköping University, SE-58183 Linköping, Sweden; per.eklund@liu.se

* Correspondence: ydu@sit.edu.cn; Tel.: +86-1821-701-7450

Received: 23 March 2019; Accepted: 28 May 2019; Published: 24 June 2019



Abstract: Reduced graphene oxide (rGO)/Bi₂Te₃ nanocomposite powders with different contents of rGO have been synthesized by a one-step *in-situ* reductive method. Then, rGO/Bi₂Te₃ nanocomposite bulk materials were fabricated by a hot-pressing process. The effect of rGO contents on the composition, microstructure, TE properties, and carrier transportation of the nanocomposite bulk materials has been investigated. All the composite bulk materials show negative Seebeck coefficient, indicating n-type conduction. The electrical conductivity for all the rGO/Bi₂Te₃ nanocomposite bulk materials decreased with increasing measurement temperature from 25 °C to 300 °C, while the absolute value of Seebeck coefficient first increased and then decreased. As a result, the power factor of the bulk materials first increased and then decreased, and a power factor of 1340 μWm⁻¹K⁻² was achieved for the nanocomposite bulk materials with 0.25 wt% rGO at 150 °C.

Keywords: reduced graphene oxide; Bi₂Te₃; composite; thermoelectric

1. Introduction

Thermoelectric (TE) materials directly convert waste heat into electrical energy [1]. The TE properties of a TE material can be estimated by the figure of merit, $ZT = S^2\sigma T/\kappa$, where S is the Seebeck coefficient, σ is the electrical conductivity, T is the absolute temperature, and κ is the total thermal conductivity (the sum of electronic and lattice (or phonon) contributions) [2,3]. Decreasing the material dimensionality is an effective method to enhance its ZT value by optimizing the S , σ , and κ , which has been proven by both theoretical research and experimental research [4–8]. For example, the ZT value of Bi₂Te₃-based alloys has been significantly enhanced by decreasing its dimensionality [6,7,9].

Carbon nanotubes and graphene have shown high electrical conductivity, high carrier mobility, and high mechanical properties [10,11], and have been widely used in the research on inorganic TE composite materials [12–19]. For example, Dong et al. [12] prepared PbTe/graphene nanocomposite powders by a wet chemical method, and then sintered the as-prepared powders by a spark plasma sintering (SPS) process at 580 °C, and a ZT value of 0.7 was obtained at 670 K for the composite with 5% mass ratio of graphene: PbTe. Ju et al. [13] fabricated Bi₂Te₃ nanowire (NW)/graphene composite films by wet chemical synthesis combined with a sintering process, and a ZT value of 0.2 was obtained for the composite film with 20 wt% Bi₂Te₃ NWs at 300 K. Liang et al. [14] prepared Bi₂Te₃/graphene bulk materials by a hydrothermal process combining SPS method, and a ZT value of 0.21 was obtained for the composite with 0.2 vol.% graphene at 475 K. Agarwal et al. [15] prepared Bi₂Te₃/graphene bulk materials by a cold pressing method, and a ZT value of 0.92 was obtained for the composite with 0.05 wt% graphene at 402 K. Kumar et al. [16] synthesized Bi₂Te₃/reduced graphene oxide (rGO) nanocomposites by a refluxing method, and then pressed the as-prepared nanocomposites into pellets; a ZT value of ~0.35 was obtained for the pellet at ~340 K. Zhang et al. [17] reported Bi_{0.4}Sb_{1.6}Te₃ bulk

materials by a high-pressure and high-temperature synthesis and high pressure sintering method, and a ZT value of 1.26 at 423 K was obtained for the composite with 0.05 wt% graphene. Ju et al. [18] fabricated Bi_2Te_3 NW/graphene bulk materials by a wet-chemical synthetic route and subsequent sintering process, and a ZT value of 0.4 was obtained for the composite with 1 wt% graphene at 300 K. Shin et al. [19] prepared $\text{rGO}/\text{Bi}_{0.36}\text{Sb}_{1.64}\text{Te}_3$ composites by a melt spinning process combining SPS method, and a ZT value of 1.16 was achieved for the composite with 0.4 vol.% rGO at 393 K.

However, systematic research about the influence of rGO content on the morphologies, TE properties, especially on the carrier transportation of $\text{rGO}/\text{Bi}_2\text{Te}_3$ bulk materials, are very limited. In this work, $\text{rGO}/\text{Bi}_2\text{Te}_3$ nanocomposite powders with different contents of rGO were synthesized by a one-step *in-situ* reductive method, and then $\text{rGO}/\text{Bi}_2\text{Te}_3$ nanocomposite bulk materials were fabricated by a hot-pressing method. The effect of rGO content on the composition, microstructure, TE properties, and carrier transportation of the nanocomposite bulk materials have been investigated.

2. Materials and Methods

2.1. Materials

Sodium tartrate ($\text{C}_4\text{H}_4\text{Na}_2\text{O}_6 \cdot 2\text{H}_2\text{O}$, ACS reagent) was purchased from Sigma-Aldrich. Tellurium dioxide (TeO_2 , guaranteed reagent) and potassium borohydride (KBH_4 , analytical reagent) were purchased from Adamas Reagent Co., Ltd. Bismuth nitrate pentahydrate ($\text{Bi}(\text{NO}_3)_3 \cdot 5\text{H}_2\text{O}$, analytical reagent) and absolute ethanol ($\text{C}_2\text{H}_5\text{OH}$, reagent grade) were purchased from Sinopharm Chemical Reagent Co., Ltd. Potassium hydroxide (KOH , analytical reagent) was purchased from General Reagent Co., Ltd. Graphene oxide (thickness: 0.8–1.2 nm) was purchased from Nanjing XFNANO Materials Tech Co., Ltd. All the materials were used without further treatment or purification.

2.2. Preparation of $\text{rGO}/\text{Bi}_2\text{Te}_3$ Nanocomposite Powders

Typical synthetic process of $\text{rGO}/\text{Bi}_2\text{Te}_3$ nanocomposite powders is as follows: a designed amount of graphene oxide (GO) was dispersed in 80 mL deionized water and then ultrasonicated for 1 h to form the transparent GO dispersion solution (Solution A). 2 g $\text{C}_4\text{H}_4\text{Na}_2\text{O}_6 \cdot 2\text{H}_2\text{O}$, 0.48 g TeO_2 , and 4.5 g KOH were added successively to the Solution A and stirred for 30 min to form Solution B. 0.97 g $\text{Bi}(\text{NO}_3)_3 \cdot 5\text{H}_2\text{O}$ was added into the Solution B and stirred for 2 h to form Solution C. 1.2 g KBH_4 as reducing agent was added into the Solution C and stirred for 30 min (Solution D). After that, Solution D was transferred to the sealed Teflon-lined autoclave and heated at 180 °C for 24 h, and then naturally cooled to the room temperature. Finally, the product was dried in vacuum at 60 °C for 6 h after washing by deionized water and absolute ethyl alcohol for several times. The weight percent (nominal composition) of rGO in the $\text{rGO}/\text{Bi}_2\text{Te}_3$ nanocomposite powders was 0.25 wt%, 0.5 wt%, and 1 wt%, respectively. The pure Bi_2Te_3 nanoparticles were prepared by the same procedure without adding GO. The rGO was prepared by the same procedure without adding $\text{C}_4\text{H}_4\text{Na}_2\text{O}_6 \cdot 2\text{H}_2\text{O}$, TeO_2 , KOH , or $\text{Bi}(\text{NO}_3)_3 \cdot 5\text{H}_2\text{O}$. The $\text{rGO}/\text{Bi}_2\text{Te}_3$ nanocomposite powders with different content of rGO were hot-pressed into pellets in a graphite die (12.7 mm in diameter) at 648 K and 80 MPa for 2 h under vacuum. The thickness of the as-prepared $\text{rGO}/\text{Bi}_2\text{Te}_3$ nanocomposite bulk materials is ~1.5 mm. Figure 1 illustrates the procedure for preparation of $\text{rGO}/\text{Bi}_2\text{Te}_3$ nanocomposite bulk materials.

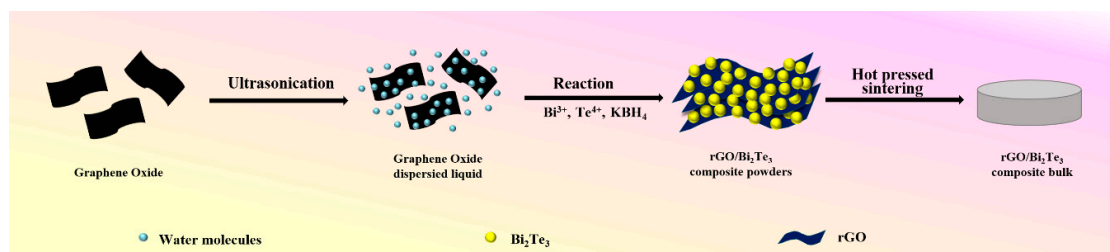


Figure 1. Preparation of $\text{rGO}/\text{Bi}_2\text{Te}_3$ nanocomposite bulk materials.

2.3. Sample Characterization

The compositions of samples were characterized by X-ray powder diffraction (XRD, Bruker D8 Advance, Karlsruhe, Germany) and Raman spectroscopy with 532 nm laser excitation (Thermo Fisher DXR, USA). The morphologies of samples were characterized using scanning electron microscopy (SEM, Philips XL 30 FEG, Philips, Eindhoven, The Netherlands) and transmission electron microscopy (TEM, Technai G2 F20, FEI, USA). The Seebeck coefficient was determined from the slope of the voltage vs temperature gradients of 0–5 K. The resistivity and Hall coefficient were measured by the van der Pauw technique. The Hall coefficient measurement was carried out under a reversible magnetic field of 1.5 T [20]. The total thermal conductivity (κ) of the composites was estimated with the relationship $\kappa = \alpha \cdot \rho \cdot C_p$, where α is thermal diffusivity, ρ is bulk density, and C_p is the specific heat of the material [21,22]. Note that the thermal conductivity will be used for the total thermal conductivity in the rest of the paper unless otherwise specified. The α and C_p were measured using LFA 467 (NETZSCH) from RT to 300 °C in Ar. The ρ was measured by the Archimedes method [23,24]. The relative density of the rGO/Bi₂Te₃ nanocomposite bulk materials with different content of rGO was calculated by the ratio of the corresponding measured density: theoretical density. The density of Bi₂Te₃ and rGO used for calculating the theoretical density of the rGO/Bi₂Te₃ bulk material was 7.86 g/cm³ [14] and 2.28 g/cm³ [25], respectively.

3. Results and Discussion

Figure 2 shows the XRD patterns of rGO/Bi₂Te₃ nanocomposite powders with different contents of rGO from 0 to 1 wt%. All the peaks of the as-prepared Bi₂Te₃ nanoparticles and rGO/Bi₂Te₃ nanocomposite powders can be indexed to the single phase Bi₂Te₃ (JCPDF, No. 15-0863). The peaks at $2\theta = 17.4^\circ, 23.6^\circ, 27.6^\circ, 37.8^\circ, 41.1^\circ, 45.2^\circ, 50.2^\circ, 57.1^\circ, 62.2^\circ$, and 66.8° are attributed to the (006), (101), (015), (1010), (110), (0015), (205), (0210), (1115), and (125) planes of Bi₂Te₃, respectively. It can be seen that as the content of rGO is increased from 0 to 1 wt%, no other peaks appear, which agrees with the results reported in Ref. [16].

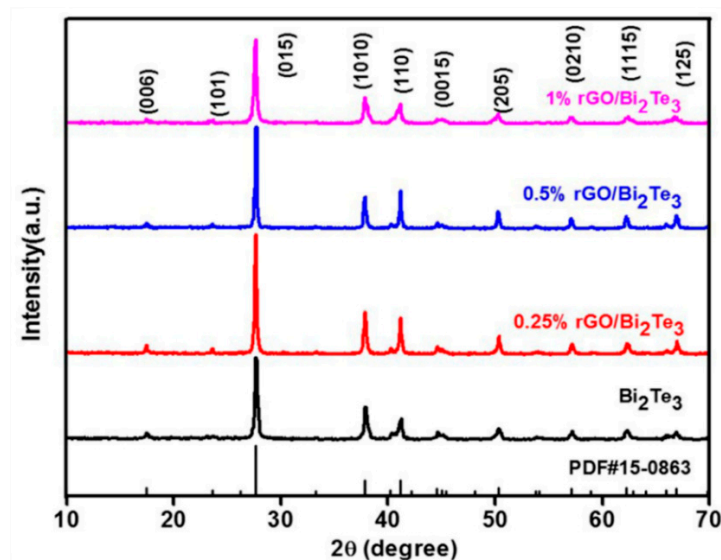


Figure 2. XRD patterns of the rGO/Bi₂Te₃ nanocomposite powders with different contents of rGO from 0 to 1 wt%.

Figure 3 shows the Raman spectra of GO, rGO, Bi₂Te₃ powders, and rGO/Bi₂Te₃ nanocomposite powders with 0.25 wt% rGO. The peaks at 1352 cm^{−1} and 1595 cm^{−1}, 1341 cm^{−1} and 1583 cm^{−1}, 1341 cm^{−1} and 1587 cm^{−1} are contributed to the D-band and G-band of GO, rGO, and rGO/Bi₂Te₃ nanocomposite powders with 0.25 wt% rGO, respectively, which agrees with the results reported in

Refs. [26,27]. The intensity of I_D/I_G increased after GO was transferred to rGO, which agrees with the results reported in the Ref. [28].

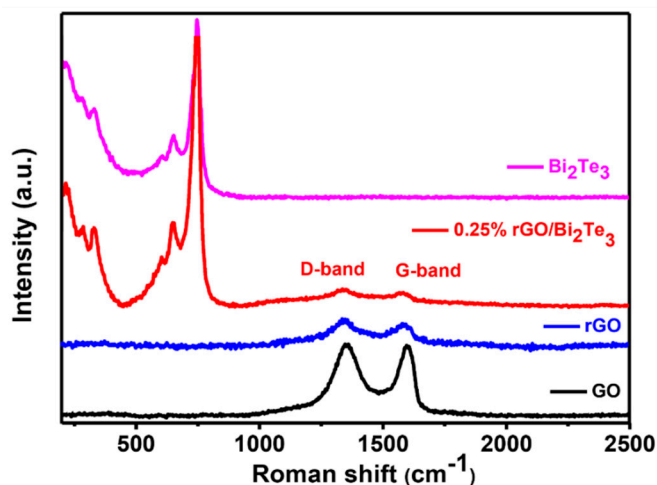


Figure 3. Raman spectra of GO, rGO, Bi_2Te_3 powders, and rGO/ Bi_2Te_3 nanocomposite powders with 0.25 wt% rGO.

Figure 4a–f shows SEM images of the rGO/ Bi_2Te_3 nanocomposite powders with different contents of rGO. Figure 4g,h shows TEM images of the rGO/ Bi_2Te_3 nanocomposite powders with 1 wt% rGO. It can be seen that the particle size of the as-prepared Bi_2Te_3 is ~50–100 nm, and Bi_2Te_3 nanoparticles are uniformly decorated on rGO layers in the nanocomposites.

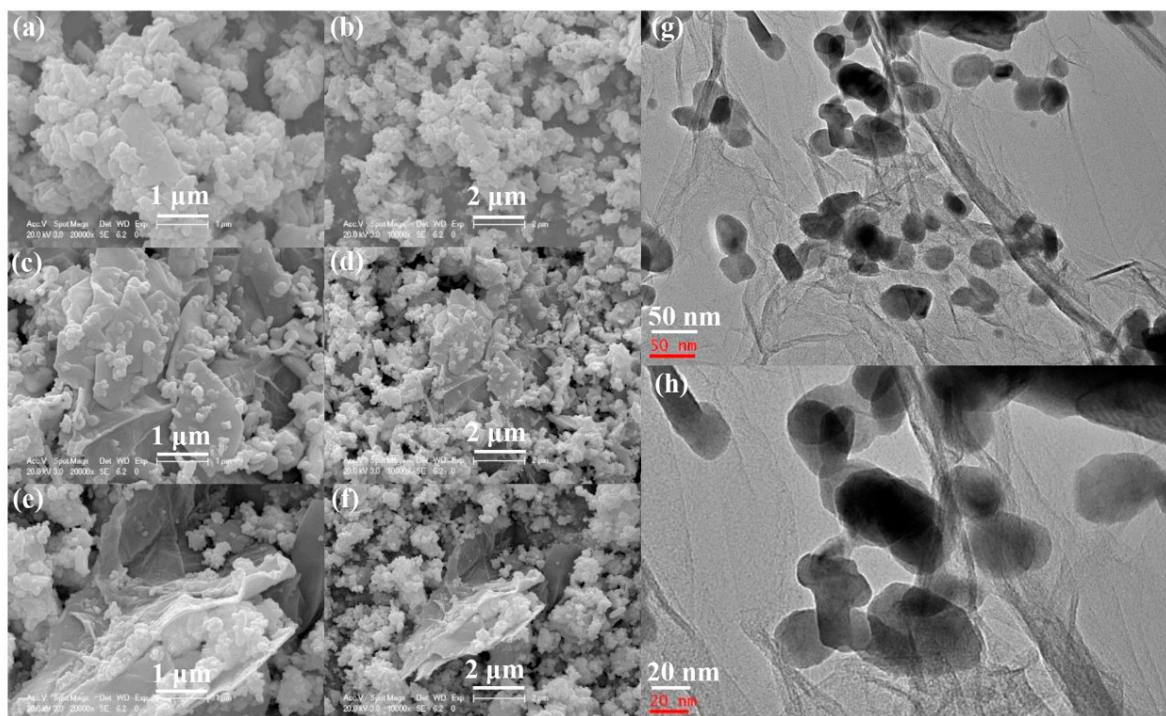


Figure 4. SEM images of rGO/ Bi_2Te_3 nanopowders with (a,b) 0.25 wt%; (c,d) 0.5 wt%; and (e,f) 1 wt% rGO; (g,h) TEM images of rGO/ Bi_2Te_3 nanopowders with 1 wt% rGO.

Figure 5 shows the XRD patterns of the rGO/ Bi_2Te_3 nanocomposite bulk material with 0.25 wt% rGO. All the peaks except the weak peaks marked by asterisks can be indexed to the single phase Bi_2Te_3 (JCPDF, No. 15-0863). The marked peaks can be indexed to Bi_2TeO_5 (JCPDF, No. 70-5000),

which is mainly due to that the powders were slightly oxidized during the hot-pressing sintering [23]. The rGO/Bi₂Te₃ composite powders were of nanosize and would adsorb oxygen on their surfaces, and the adsorbed oxygen could not be fully eliminated even the hot-pressing was carried out under vacuum [23]. The intensities of the (006) and (0015) planes for the rGO/Bi₂Te₃ nanocomposite bulk materials are significantly enhanced when compared to the powders (see Figure 2), which indicates the preferred orientation for the bulk materials after the hot-pressing sintering [29].

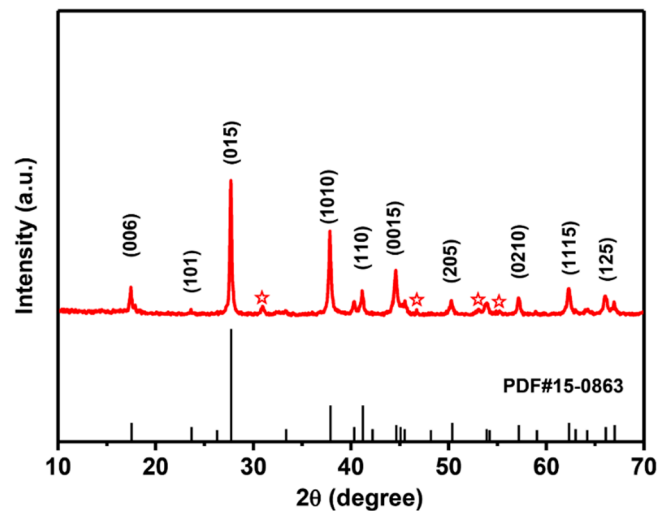


Figure 5. XRD patterns of the rGO/Bi₂Te₃ nanocomposite bulk material with 0.25 wt% rGO.

Figure 6a–c shows SEM images of the fracture surface of rGO/Bi₂Te₃ nanocomposite bulk materials with different contents of rGO prepared by a hot-pressing method, and Figure 6d–f shows the corresponding energy dispersive X-ray spectrometry (EDS) mappings of C, Te, and Bi, respectively for the sample in Figure 6c. It can be seen that the rGO is sandwiched by Bi₂Te₃ particles in the nanocomposites. The relative density of rGO/Bi₂Te₃ composite bulk materials with 0, 0.25 wt%, 0.5 wt%, and 1 wt% of rGO was 94.28%, 94.12%, 93.05%, and 90.61%, respectively.

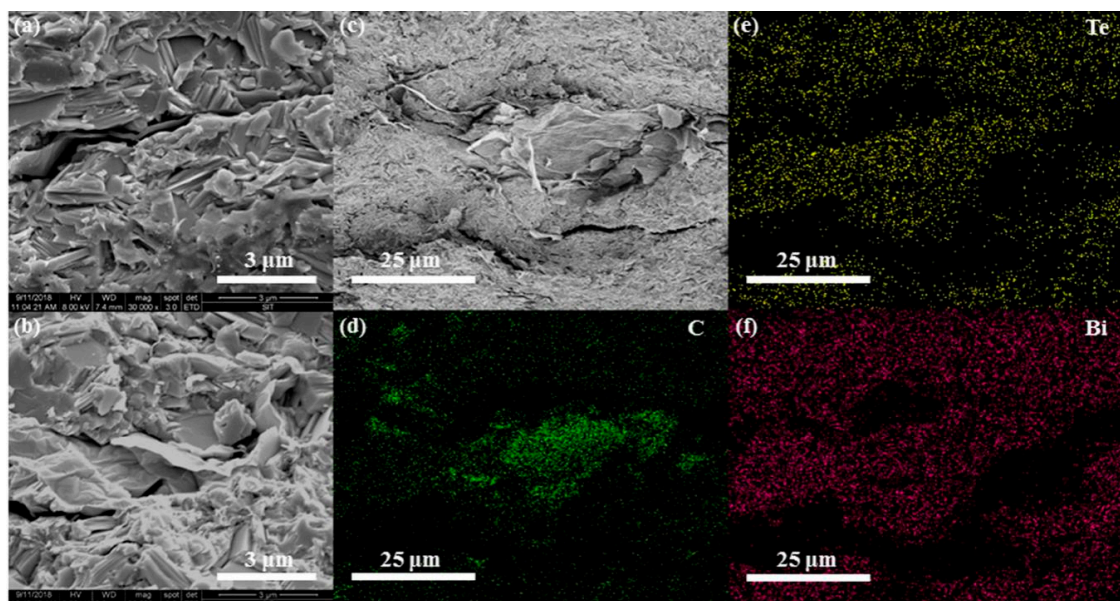


Figure 6. SEM images of rGO/Bi₂Te₃ nanocomposite bulk materials with (a) 0.25 wt%; (b) 0.5 wt%; and (c) 1 wt% rGO; (d–f) are the corresponding SEM-EDS mapping images (C, Te, and Bi element) of the panel (c), respectively.

The transport properties of the rGO/Bi₂Te₃ nanocomposite bulk materials with different contents of rGO are plotted in Figure 7a–e. The electrical conductivities for all the rGO/Bi₂Te₃ nanocomposite bulk materials are lower than that of pure Bi₂Te₃ bulk materials. As the content of rGO is increased from 0 to 1 wt%, the electrical conductivity of the rGO/Bi₂Te₃ nanocomposite bulk materials decreases from 1403 S/cm to 1025 S/cm at room temperature. These values are higher than those of typical values for Bi₂Te₃/graphene bulk material (~950 S/cm with 0.2 vol.% graphene at 300 K) [14] or Bi₂Te₃ NW/graphene bulk material (~230 S/cm with 1 wt% graphene at 300 K) [18], but very close to Bi₂Te₃/rGO bulk material (1440 S/cm at 300 K) [16]. The electrical conductivity for all the samples decreased as the measurement temperature was increased from 25 °C to 300 °C, indicative of degenerate semiconductor behavior [30].

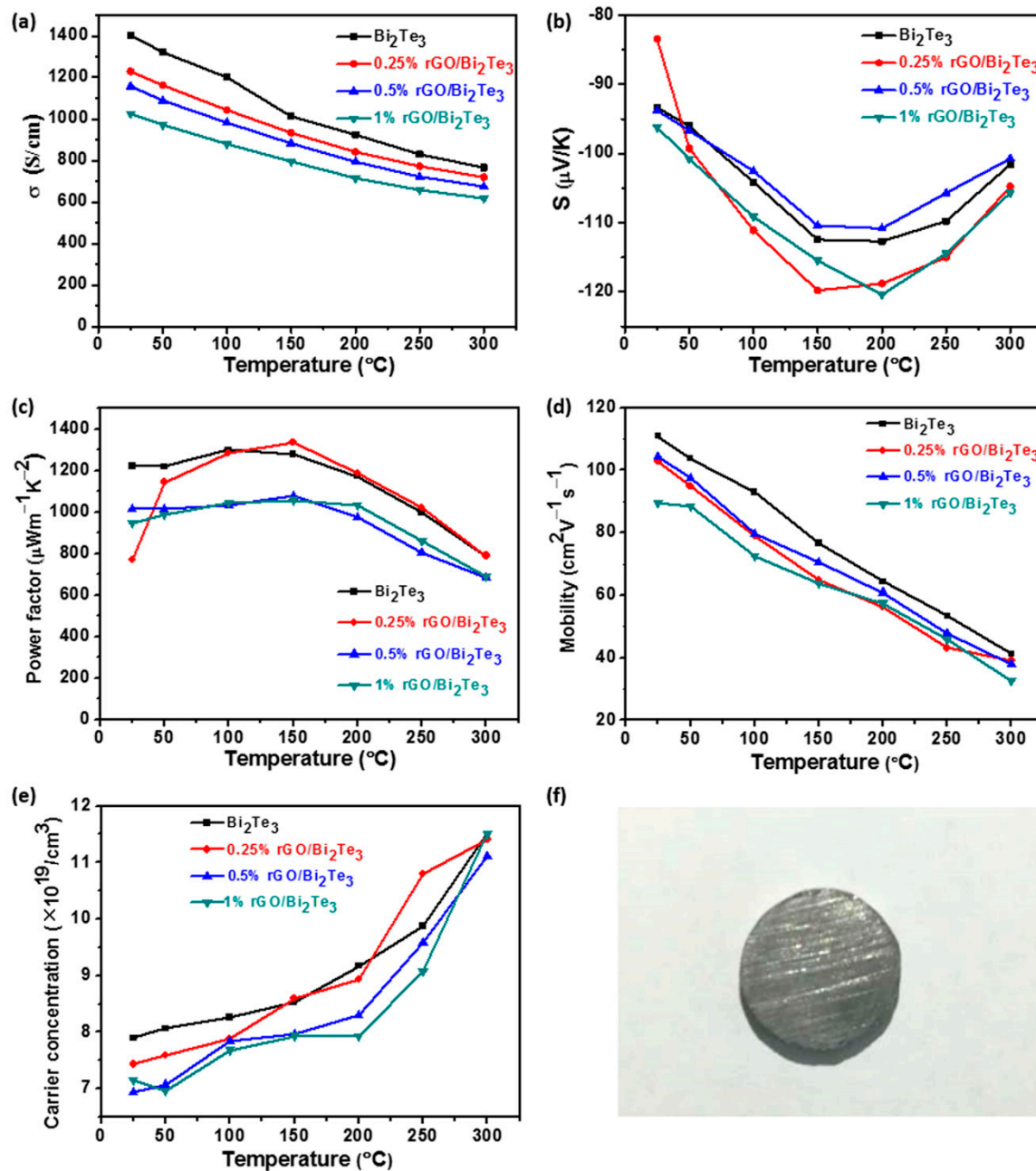


Figure 7. Temperature dependent (a) electrical conductivity; (b) Seebeck coefficient; (c) power factor; (d) carrier mobility; and (e) carrier concentration of rGO/Bi₂Te₃ nanocomposite bulk materials with different contents of rGO from 0 to 1 wt%; (f) Digital photo of rGO/Bi₂Te₃ nanocomposite bulk materials with 1 wt% rGO.

All the bulk materials have negative Seebeck coefficient, indicating n-type conduction (Figure 7b). As the measurement temperature increased, the absolute value of Seebeck coefficient for all the samples first increased and then decreased, e.g., the absolute value of the (negative) Seebeck coefficient of the composite with 1 wt% rGO increased from 96 $\mu\text{V/K}$ at 25 $^{\circ}\text{C}$ to 120 $\mu\text{V/K}$ at 200 $^{\circ}\text{C}$, and then decreased to 105 $\mu\text{V/K}$ at 300 $^{\circ}\text{C}$. The absolute value of the (negative) Seebeck coefficient of the composite with 1 wt% rGO (96 $\mu\text{V/K}$ at 25 $^{\circ}\text{C}$) is higher than that of a $\text{Bi}_2\text{Te}_3/\text{rGO}$ bulk material (83 $\mu\text{V/K}$ at 300 K) [16]; however, it is lower than that of a $\text{Bi}_2\text{Te}_3/\text{graphene}$ bulk material ($\sim 113 \mu\text{V/K}$ with 0.2 vol.% graphene at 475 K) [14] and a $\text{Bi}_2\text{Te}_3 \text{ NW/graphene}$ bulk material ($\sim 170 \mu\text{V/K}$ with 1 wt% graphene at 300 K) [18].

The power factor of the samples first increased and then decreased as the measurement temperature was increased from 25 $^{\circ}\text{C}$ to 300 $^{\circ}\text{C}$ (Figure 7c), mainly due to the same trend of the absolute value of Seebeck coefficient and the decreased electrical conductivity. A power factor of 1340 $\mu\text{Wm}^{-1}\text{K}^{-2}$ was achieved for the composites with 0.25 wt% rGO at 150 $^{\circ}\text{C}$. This value is much higher than that of a $\text{Bi}_2\text{Te}_3/\text{graphene}$ film with 80 wt% graphene ($\sim 480 \mu\text{Wm}^{-1}\text{K}^{-2}$ at 300 K) [13], a $\text{Bi}_2\text{Te}_3/\text{graphene}$ bulk material with 0.2 vol.% graphene ($\sim 1000 \mu\text{Wm}^{-1}\text{K}^{-2}$ at 475 K) [14], and a $\text{Bi}_2\text{Te}_3 \text{ NW/graphene}$ bulk material with 1 wt% graphene ($\sim 650 \mu\text{Wm}^{-1}\text{K}^{-2}$ at 300 K) [18].

To explain the effect of rGO content and temperature on the electrical conductivity and Seebeck coefficient of the bulk composites, the carrier mobility and carrier concentration of the bulk composites were determined, and are shown in Figure 7d–e. The electrical conductivity of materials can be calculated by the following equation [31].

$$\sigma = ne\mu, \quad (1)$$

where σ is the electrical conductivity, n is the carrier concentration, e is the charge of electron, and μ is the carrier mobility. It can be seen that as the content of rGO is increased from 0 to 1 wt%, both the carrier mobility and the carrier concentration of the bulk composites decreased somewhat. As the measurement temperature was increased from 25 $^{\circ}\text{C}$ to 300 $^{\circ}\text{C}$, the carrier mobility decreased, while the carrier concentration increased. The decrease in carrier mobility is much larger than the increase in carrier concentration, which leads to a significant decrease of the electrical conductivity.

The Seebeck coefficient for metals and degenerate semiconductors can be expressed by the following equation [32].

$$S = m^*T \frac{8\pi^2 k_B^2}{3eh^2} \left(\frac{\pi}{3n} \right)^{\frac{2}{3}}, \quad (2)$$

where m^* is the effective mass of the carrier, h is the Planck constant, and k_B is the Boltzmann constant. The carrier scattering and the carrier concentration are significantly affect the Seebeck coefficient of the composites. As the measurement temperature was increased, the absolute value of Seebeck coefficient for all the samples first increased and then decreased, which agrees with the results reported in the Ref. [14]. This phenomenon is mainly due to the combined effects by the increased amount of interfaces between the rGO and Bi_2Te_3 nanoparticles, correlated decreased carrier mobility and increased carrier concentration as the temperature increased from 25 $^{\circ}\text{C}$ to 300 $^{\circ}\text{C}$.

Normally, the thermal conductivities of Bi_2Te_3 bulk materials and $\text{rGO}/\text{Bi}_2\text{Te}_3$ bulk materials are in the range of 0.55–3.0 $\text{Wm}^{-1}\text{K}^{-1}$ and 0.45–3.9 $\text{Wm}^{-1}\text{K}^{-1}$ at room temperature, respectively [13,14,16,18]. As 1340 $\mu\text{Wm}^{-1}\text{K}^{-2}$ was the highest power factor achieved for the nanocomposite bulk materials with 0.25 wt% rGO at 150 $^{\circ}\text{C}$ in this work, the thermal conductivity of $\text{rGO}/\text{Bi}_2\text{Te}_3$ bulk material with 0.25 wt% rGO was measured, and the thermal conductivity of Bi_2Te_3 bulk material was also measured for a comparison (see Figure 8). The thermal conductivity of the samples agrees with the results reported in Refs. [13,14,16,18]. The thermal conductivity of Bi_2Te_3 bulk materials decreased after the addition of rGO, e.g., from 1.46 $\text{Wm}^{-1}\text{K}^{-1}$ for Bi_2Te_3 bulk materials to 1.34 $\text{Wm}^{-1}\text{K}^{-1}$ for $\text{rGO}/\text{Bi}_2\text{Te}_3$ bulk materials with 0.25 wt% rGO at room temperature. The decrease in the thermal conductivity mainly due to the interfaces between the rGO and Bi_2Te_3 existed in the composites (see Figure 6), which affected the carrier scattering, and then decreased the thermal conductivity.

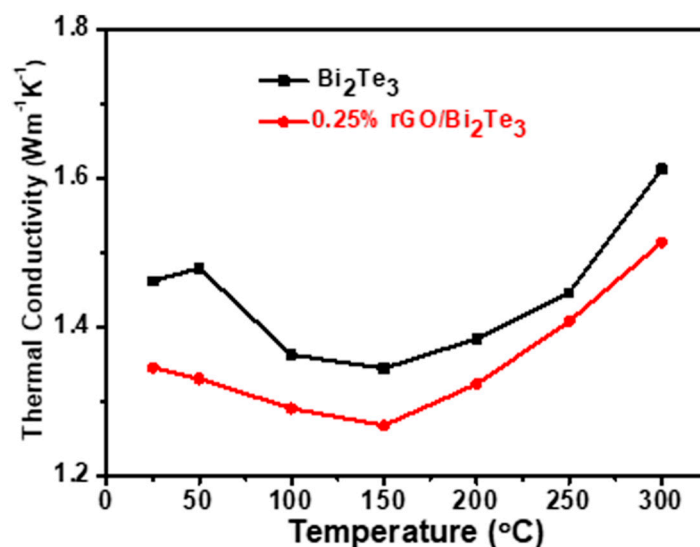


Figure 8. The thermal conductivity (κ) of Bi₂Te₃ bulk materials and rGO/Bi₂Te₃ nanocomposite bulk materials with 0.25 wt% rGO (parallel to the hot-pressing sintering direction).

As the electrical conductivity and thermal conductivity were measured in different directions, the ZT value curves of the samples were not presented. According to the ratio of 1.5 for the thermal conductivity (perpendicular to the hot-pressing sintering direction: parallel to the hot-pressing sintering direction) of the Bi₂Te_{2.7}Se_{0.3} bulk material [33], a ZT value of ~ 0.3 at 150 °C for rGO/Bi₂Te₃ composite bulk material with 0.25 wt% was estimated.

Both the as-prepared rGO/Bi₂Te₃ nanocomposite powders and bulk materials have great potential to be used for TE devices. The rGO/Bi₂Te₃ bulk materials can be cut into suitable size and then assembled to flexible TE devices on flexible substrates (e.g., polyimide or polyethylene terephthalate substrates) [34] or traditional TE devices on rigid inorganic substrates (e.g., ceramic substrate) [35], respectively. The rGO/Bi₂Te₃ nanocomposite powders can be dispersed in suitable solvents and then to prepare composite films by a vacuum filtration method [36] or used as active materials to prepare slurry and then to fabricate composite film by a dispenser printing technique [37]. The as-prepared composites films can be used for fabrication of flexible TE devices [2]. Therefore, this work lays a foundation and is essential for fabrication of TE devices. The applications of rGO/Bi₂Te₃ composite powders and bulk materials on TE devices are under investigation.

4. Conclusions

Reduced graphene oxide (rGO)/Bi₂Te₃ nanocomposite bulk materials were prepared by hot-pressing of rGO/Bi₂Te₃ nanocomposite powders, which were fabricated by a one-step *in-situ* reductive method. As the measured temperature increased from 25 °C to 300 °C, the power factor of the samples first increased and then decreased, mainly due to the similar trend of the absolute value of Seebeck coefficient and decreased electrical conductivity. A power factor of 1340 $\mu\text{Wm}^{-1}\text{K}^{-2}$ was achieved for the composites with 0.25 wt% rGO at 150 °C.

Author Contributions: Y.D. designed the experiments, performed data analysis, and wrote and revised the manuscript; J.L. performed the experiments, data analysis, and wrote the manuscript; J.X. and P.E. revised the manuscript and provided additional intellectual insight; Y.D. conceived the overall project.

Acknowledgments: This work has been supported by the National Natural Science Foundation of China (61504081, 11811530636, 61611530550), the Shanghai Innovation Action Plan Project (17090503600), and the Program for Professor of Special Appointment (Young Eastern Scholar Program) at Shanghai Institutions of Higher Learning (QD2015039). P.E. also acknowledges the Knut and Alice Wallenberg Foundation for an Academy Fellow grant and the Swedish Energy Agency under project grant 46519-1.

Conflicts of Interest: The authors declare no conflict of interest.

References

1. Poudel, B.; Hao, Q.; Ma, Y.; Lan, Y.C.; Minnich, A.; Yu, B.; Yan, X.; Wang, D.Z.; Muto, A.; Vashaee, D.; et al. High-thermoelectric performance of nanostructured bismuth antimony telluride bulk alloys. *Science* **2008**, *320*, 634–638. [\[CrossRef\]](#)
2. Du, Y.; Xu, J.Y.; Paul, B.; Eklund, P. Flexible thermoelectric materials and devices. *Appl. Mater. Today* **2018**, *12*, 366–388. [\[CrossRef\]](#)
3. Chung, D.Y.; Hogan, T.; Brazis, P.; Rocci-Lane, M.; Kannewurf, C.; Bastea, M.; Uher, C.; Kanatzidis, M.G. CsBi_4Te_6 : A high-performance thermoelectric material for low-temperature applications. *Science* **2000**, *287*, 1024–1027. [\[CrossRef\]](#)
4. Hicks, L.D.; Dresselhaus, M.S. Thermoelectric figure of merit of a one-dimensional conductor. *Phys. Rev. B* **1993**, *47*, 16631–16634. [\[CrossRef\]](#)
5. Hicks, L.D.; Harman, T.C.; Sun, X.; Dresselhaus, M.S. Experimental study of the effect of quantum-well structures on the thermoelectric figure of merit. *Phys. Rev. B* **1996**, *53*, R10493–R10496. [\[CrossRef\]](#)
6. Venkatasubramanian, R.; Siivola, E.; Colpitts, T.; O’Quinn, B. Thin-film thermoelectric devices with high room-temperature figures of merit. *Nature* **2001**, *413*, 597–602. [\[CrossRef\]](#)
7. Xie, W.J.; Tang, X.F.; Yan, Y.G.; Zhang, Q.J.; Tritt, T.M. Unique nanostructures and enhanced thermoelectric performance of melt-spun BiSbTe alloys. *Appl. Phys. Lett.* **2009**, *94*, 102111. [\[CrossRef\]](#)
8. Du, Y.; Shen, S.Z.; Cai, K.F.; Casey, P.S. Research progress on polymer-inorganic thermoelectric nanocomposite materials. *Prog. Polym. Sci.* **2012**, *37*, 820–841. [\[CrossRef\]](#)
9. Hung, N.T.; Hasdeo, E.H.; Nugraha, A.R.T.; Dresselhaus, M.S.; Saito, R. Quantum effects in the thermoelectric power factor of low-dimensional semiconductors. *Phys. Rev. Lett.* **2016**, *117*, 036602. [\[CrossRef\]](#)
10. Du, Y.; Shen, S.Z.; Yang, W.D.; Donelson, R.; Cai, K.F.; Casey, P.S. Simultaneous increase in conductivity and Seebeck coefficient in a polyaniline/graphene nanosheets thermoelectric nanocomposite. *Synth. Met.* **2012**, *161*, 2688–2692. [\[CrossRef\]](#)
11. Jin, Q.; Jiang, S.; Zhao, Y.; Wang, D.; Qiu, J.H.; Tang, D.M.; Tan, J.; Sun, D.M.; Hou, P.X.; Chen, X.Q.; et al. Flexible layer-structured Bi_2Te_3 thermoelectric on a carbon nanotube scaffold. *Nat. Mater.* **2019**, *18*, 62–68. [\[CrossRef\]](#) [\[PubMed\]](#)
12. Dong, J.D.; Liu, W.; Han, L.; Su, X.L.; Tang, X.F.; Uher, C. In situ synthesis and thermoelectric properties of PbTe -graphene nanocomposites by utilizing a facile and novel wet chemical method. *J. Mater. Chem. A* **2013**, *1*, 12503–12511. [\[CrossRef\]](#)
13. Ju, H.; Kim, M.; Kim, J. A facile fabrication of n-type Bi_2Te_3 nanowire/graphene layer-by-layer hybrid structures and their improved thermoelectric performance. *Chem. Eng. J.* **2015**, *275*, 102–112. [\[CrossRef\]](#)
14. Liang, B.B.; Song, Z.J.; Wang, M.H.; Wang, L.J.; Jiang, W. Fabrication and thermoelectric properties of graphene/composite materials. *J. Nanomater.* **2013**, *2013*, 1–5.
15. Agarwal, K.; Kaushik, V.; Varandani, D.; Dhar, A.; Mehta, B.R. Nanoscale thermoelectric properties of Bi_2Te_3 -graphene nanocomposites: Conducting atomic force, scanning thermal and kelvin probe microscopy studies. *J. Alloys Compd.* **2016**, *681*, 394–401. [\[CrossRef\]](#)
16. Kumar, S.; Singh, S.; Dhawan, P.K.; Yadav, R.R.; Khare, N. Effect of graphene nanofillers on the enhanced thermoelectric properties of Bi_2Te_3 nanosheets: Elucidating the role of interface in de-coupling the electrical and thermal characteristics. *Nanotechnology* **2018**, *29*, 135703. [\[CrossRef\]](#) [\[PubMed\]](#)
17. Zhang, Y.W.; Ma, H.; Sun, B.; Liu, B.W.; Liu, H.Q.; Kong, L.J.; Liu, B.M.; Jia, X.P.; Chen, X. Thermoelectric performance of graphene composited BiSbTe bulks by high pressure synthesis. *J. Alloys Compd.* **2017**, *715*, 344–348. [\[CrossRef\]](#)
18. Ju, H.; Kim, J. Preparation and structure dependent thermoelectric properties of nanostructured bulk bismuth telluride with graphene. *J. Alloys Compd.* **2016**, *664*, 639–647. [\[CrossRef\]](#)
19. Shin, W.H.; Ahn, K.; Jeong, M.; Yoon, J.S.; Song, J.M.; Lee, S.; Seo, W.S.; Lim, Y.S. Enhanced thermoelectric performance of reduced graphene oxide incorporated bismuth-antimony-telluride by lattice thermal conductivity reduction. *J. Alloys Compd.* **2017**, *718*, 342–348. [\[CrossRef\]](#)
20. Li, J.; Chen, Z.W.; Zhang, X.Y.; Sun, Y.X.; Yang, J.; Pei, Y.Z. Electronic origin of the high thermoelectric performance of GeTe among the p-type group IV monotellurides. *NPG Asia Mater.* **2017**, *9*, e353. [\[CrossRef\]](#)
21. Vaney, J.B.; Yamini, S.A.; Takaki, H.; Kobayashi, K.; Kobayashi, N.; Mori, T. Magnetism-mediated thermoelectric performance of the Cr-doped bismuth telluride tetradymite. *Mater. Today Phys.* **2019**, *9*, 100090. [\[CrossRef\]](#)

22. Feng, C.P.; Bai, L.; Shao, Y.; Bao, R.Y.; Liu, Z.Y.; Yang, M.B.; Chen, J.; Ni, H.Y.; Yang, W. A facile route to fabricate highly anisotropic thermally conductive elastomeric POE/NG composites for thermal management. *Adv. Mater. Interfaces* **2018**, *5*, 1700946. [\[CrossRef\]](#)
23. Du, Y.; Cai, K.F.; Li, H.; An, B.J. The influence of sintering temperature on the microstructure and thermoelectric properties of n-Type $\text{Bi}_2\text{Te}_{3-x}\text{S}_x$ nanomaterials. *J. Electron. Mater.* **2011**, *40*, 518–522. [\[CrossRef\]](#)
24. Pan, Y.; Wei, T.R.; Cao, Q.; Li, J.F. Mechanically enhanced p-and n-type Bi_2Te_3 -based thermoelectric materials reprocessed from commercial ingots by ball milling and spark plasma sintering. *Mater. Sci. Eng. B* **2015**, *197*, 75–81. [\[CrossRef\]](#)
25. Zhou, W.Z.; Dong, M.Q.; Zhou, Z.X.; Sun, X.H.; Kikuchi, K.; Nomura, N.; Kawasaki, A. In situ formation of uniformly dispersed Al_4C_3 nanorods during additive manufacturing of graphene oxide/Al mixed powders. *Carbon* **2019**, *141*, 67–75. [\[CrossRef\]](#)
26. Tang, H.C.; Yang, C.; Lin, Z.Y.; Yang, Q.H.; Kang, F.Y.; Wong, C.P. Electro spray-deposition of graphene electrodes: a simple technique to build high-performance supercapacitors. *Nanoscale* **2015**, *20*, 9133–9139. [\[CrossRef\]](#)
27. Huang, H.; Chen, R.P.; Yang, S.Y.; Zhang, W.; Fang, Y.F.; Li, L.; Liu, Y.L.; Huang, J. High-performance Si flexible anode with rGO substrate and Ca^{2+} crosslinked sodium alginate binder for lithium ion battery. *Synth. Met.* **2019**, *247*, 212–218. [\[CrossRef\]](#)
28. Fan, Z.J.; Wang, K.; Wei, T.; Yan, J.; Song, L.P.; Shao, B. An environmentally friendly and efficient route for the reduction of graphene oxide by aluminum powder. *Carbon* **2010**, *48*, 1670–1692. [\[CrossRef\]](#)
29. Chen, L.D.; Jiang, J.; Shi, X. Thermoelectric performance of textured Bi_2Te_3 -based sintered materials prepared by spark plasma sintering. *Mater. Res. Soc. Symp. Proc.* **2003**, *793*, S9.3.1–S9.3.9. [\[CrossRef\]](#)
30. Lee, G.E.; Kim, I.H.; Choi, S.M.; Lim, Y.S.; Seo, W.S.; Park, J.S.; Yang, S.H. Process controls for Bi_2Te_3 - Sb_2Te_3 prepared by mechanical alloying and hot pressing. *J. Korean Phys. Soc.* **2014**, *65*, 2066–2070. [\[CrossRef\]](#)
31. Du, Y.; Cai, K.F.; Chen, S.; Cizek, P.; Lin, T. Facile preparation and thermoelectric properties of Bi_2Te_3 based alloy nanosheet/PEDOT:PSS composite films. *ACS Appl. Mater. Interfaces* **2014**, *6*, 5735–5743. [\[CrossRef\]](#) [\[PubMed\]](#)
32. Snyder, G.J.; Toberer, E.S. Complex thermoelectric materials. *Nat. Mater.* **2008**, *7*, 105–114. [\[CrossRef\]](#) [\[PubMed\]](#)
33. Yan, X.; Poudel, B.; Ma, Y.; Liu, W.S.; Joshi, G.; Wang, H.; Lan, Y.C.; Wang, D.Z.; Chen, G.; Ren, Z.F. Experimental studies on anisotropic thermoelectric properties and structures of n-type $\text{Bi}_2\text{Te}_{2.7}\text{Se}_{0.3}$. *Nano Lett.* **2010**, *10*, 3373–3378. [\[CrossRef\]](#) [\[PubMed\]](#)
34. Liu, H.Y.; Wang, Y.C.; Mei, D.Q.; Shi, Y.G.; Chen, Z.C. Design of a wearable thermoelectric generator for harvesting human body energy, wearable sensors and robots. In *Wearable Sensors and Robots*; Springer: Singapore, 2017; pp. 55–66.
35. Zhang, Q.H.; Huang, X.Y.; Bai, S.Q.; Shi, X.; Uher, C.; Chen, L.D. Thermoelectric devices for power generation: recent progress and future challenges. *Adv. Eng. Mater.* **2016**, *18*, 194–213. [\[CrossRef\]](#)
36. Du, Y.; Liu, X.; Xu, J.Y.; Shen, S.Z. Flexible Bi-Te-based alloy nanosheet/PEDOT:PSS thermoelectric power generators. *Mater. Chem. Front.* **2019**. [\[CrossRef\]](#)
37. Madan, D.; Chen, A.; Wright, P.K.; Evans, J.W. Printed Se-doped MA n-type Bi_2Te_3 thick-film thermoelectric generators. *J. Electron. Mater.* **2012**, *41*, 1481–1486. [\[CrossRef\]](#)

